

Primordial Black Holes in the Solar System

VALENTIN THOSS ^{1,2,3} AND ANDREAS BURKERT^{1,2,3}

¹*Universitäts-Sternwarte*

Ludwig-Maximilians-Universität München

Scheinerstr. 1

81679 Munich, Germany

²*Max-Planck-Institut für Extraterrestrische Physik*

Gießenbachstraße 1

85748 Garching, Germany

³*Excellence Cluster ORIGINS*

Boltzmannstraße 2

85748 Garching, Germany

ABSTRACT

If primordial black holes (PBHs) of asteroidal mass make up the entire dark matter they could be detectable through their gravitational influence in the solar system. In this work, we study the perturbations that PBHs induce on the orbits of planets. Detailed numerical simulations of the solar system, embedded in a halo of PBHs, are performed. Using the Earth-Mars distance as an observational probe, we show that the perturbations are below the current detection limits and thus PBHs are not directly constrained by solar system ephemerides. We estimate that an improvement in the measurement accuracy by more than an order of magnitude or the extraction of signals well below the noise level are required to detect the gravitational influence of PBHs in the solar system in the foreseeable future.

1. INTRODUCTION

Primordial black holes (PBHs) as a dark matter (DM) candidate have been studied for half a century (Carr & Green 2024), gaining special attention after the first direct detection of gravitational waves from binary black hole mergers (Abbott et al. 2016). By now, a large number of constraints have been derived that limit the fraction of dark matter that can be in the form of PBHs (Carr et al. 2021). However, these constraints come with some uncertainty and can even disappear entirely, as was recently demonstrated for light PBHs (Thoss et al. 2024; Alexandre et al. 2024).

The asteroid-mass window ($M_{\text{PBH}} \in [10^{17}, 10^{23}]$ g) has been studied with particular interest as it remains a viable parameter region for PBHs. Within this mass range, their interaction with stars, neutron stars and white dwarfs has been studied as a pathway to detect them or constrain their dark matter fraction. However, many of the bounds that were obtained in this way are disputed for various reasons (see Carr et al. (2021) for an overview).

Another approach to study PBHs of asteroidal mass is through their effect within the solar system. It has been suggested to look for craters as a signature for collisions of PBHs with moons and planets (Yalinewich & Caplan 2021; Caplan et al. 2023). Other work focuses on the gravitational effects of PBHs. This includes perturbations to the orbits of moons and planets (Li et al. 2023; Tran et al. 2023), satellite constellations (Bertrand et al. 2023) and future space-based gravitational wave detectors such as LISA (Adams & Bloom 2004; Seto & Cooray 2004). So far these are mostly proof-of-concept studies which suggest that an accurate model for solar system ephemerides, combined with a sophisticated data analysis will make the detection of individual asteroid-mass PBHs feasible. Tran et al. (2023) showed that if the extraction of signals with an amplitude of 10^{-4} relative to the noise is achieved, then one can expect to detect PBHs with a mass of $10^{18} \text{ g} < M_{\text{PBH}} < 10^{23} \text{ g}$ using already existing data.

Recently, Loeb (2024) argued that PBHs within most of the asteroid-mass window are already excluded from making up the entire dark matter, based on their perturbations of solar system bodies. The result was obtained by considering

the Poissonian fluctuation of the number of PBHs within a given radius R from the Sun. The rate of the change of the total PBH mass, enclosed within R , was compared to an observational constraint on the rate of change of the solar mass. This approach assumes that the total mass of PBHs within R has a gravitational effect similar to a point mass and therefore can be added directly to the mass of the Sun. From this, [Loeb \(2024\)](#) concluded that, for $R = 50$ AU, PBHs cannot make up the entire dark matter in the mass range $M_{\text{PBH}} \in [6 \times 10^{18}, 10^{22}]$ g. However, [Cline \(2024\)](#) has noted that the choice of $R = 50$ AU is not justified and that one cannot easily rule out PBHs as a dark matter candidate.

Because of the far-reaching consequences of the results obtained by [Loeb \(2024\)](#), it is necessary to investigate it in more detail. The key question is, whether PBHs can induce detectable perturbations on the orbits of solar system objects. In this work we present results from N-Body simulations of the solar system, embedded in a halo of PBHs. We study the perturbations that these compact objects induce on planets when crossing the solar system. Our methods are presented in Section 2 and our results are shown in Section 3. In Section 4 we provide a discussion of our results and a careful analysis of the calculation performed by [Loeb \(2024\)](#). We conclude with a summary in Section 5.

2. METHODS

Our goal is to simulate the perturbations induced on solar system objects by a halo of asteroid-mass PBHs. In this Section we briefly describe our simulation methods and relevant quantities.

We use a second-order Leapfrog integrator with a fixed timestep to simulate the motions of the Sun, the 8 planets, and the Earth's moon. Other solar system objects (SSOs) are neglected as we are only interested in the relative perturbation of planets in the solar system. The goal of this work is not to make accurate predictions on the absolute positions of the bodies of the solar system. Rather, we are interested in the relative perturbation of their position $\delta\mathbf{r}(t)$. We do not expect the smaller bodies to have a sizeable effect on these perturbations. For the same reason we do not treat finite-size effects or relativistic corrections as these will only affect the perturbations at second order. We refer to [Tran et al. \(2023\)](#) for a more detailed discussion on these effects.

The initial conditions for the SSOs are obtained from the Horizons System by JPL, based on the DE441 model ([Park et al. 2021](#)). The solar system is embedded in a halo of PBHs filling a box with periodic boundary conditions and length L_{box} . The halo is populated with $N_{\text{PBH}} = L_{\text{box}}^3 \rho_{\text{CDM}} / M_{\text{PBH}}$ PBHs of random positions, thus assuming that PBHs make up the entire dark matter with a monochromatic mass distribution. During the simulations, the gravitational forces are only computed for PBHs within a sphere of radius $R_{\text{box}} = L_{\text{box}}/2$. This makes the comparison with the case of a smooth particle dark matter component more accurate. The PBHs are given a Maxwellian velocity distribution with a dispersion $\sigma_v = 185 \text{ km s}^{-1}$ as well as an additional component due to the rotation of the galactic disk. The latter has a magnitude of $v_{\odot} = 230 \text{ km s}^{-1}$, an angle of 60° w.r.t. the ecliptic plane and a direction such that the relative motion between the PBHs and Earth is maximal on June 1st ([Freese et al. 2013](#)). These parameters lead to a relative velocity of the PBHs of $v_{\text{rms}} \approx 279 \text{ km s}^{-1} \approx 59 \text{ AU yr}^{-1}$. $\rho_{\text{CDM}} = 7 \times 10^{-25} \text{ g cm}^{-3}$ is assumed to facilitate comparisons with [Loeb \(2024\)](#).

To investigate the parameter space of the asteroid-mass window we choose $M_{\text{PBH}} \in [10^{18}, 10^{19}, 10^{20}, 10^{21}]$ g. Note that we discuss how our results can be extrapolated to other PBH masses. For each value of the mass M_{PBH} a large number of simulation runs ($\mathcal{O}(1000)$, see Table 1) are performed, each over a physical time span of 1 yr, to account for the randomness of the encounters with the solar system bodies. A smaller number of simulations are carried out over a time of 20 yr, which is roughly the time span for which the most precise ranging data in the solar system has been available. We checked for each value of M_{PBH} that both the numerical timestep and the value of R_{box} do not significantly affect our results. To reduce computational cost, the gravitational force is only calculated for the solar system bodies, whereas the PBHs move on straight trajectories. This is a reasonable approximation due to the high velocity of the PBHs. We nevertheless performed additional simulations including the gravitational force for the PBHs and found that it only changes our results below the percent-level. The exact parameters of our simulation ensemble can be found in Table 1.

The main quantity of interest is the perturbation that the PBHs induce on the distance between the Earth and a given solar system object (SSO),

$$\frac{\delta r}{r}(t) = \frac{|\tilde{\mathbf{r}}_{\text{earth}}(t) - \tilde{\mathbf{r}}_{\text{SSO}}(t)| - |\mathbf{r}_{\text{earth}}(t) - \mathbf{r}_{\text{SSO}}(t)|}{|\mathbf{r}_{\text{earth}}(t) - \mathbf{r}_{\text{SSO}}(t)|}, \quad (1)$$

where $\tilde{\mathbf{r}}$ indicates the position in a simulation with PBHs and \mathbf{r} refers to the comparative simulation with a smooth DM halo. Naively, one might assume that the comparative simulation setup must be a solar system without dark

M_{PBH} (g)	N_{PBH}	R_{box} (AU)	N_{runs}	t (yr)
10^{18}	18525	200	1000	1
10^{19}	6252	300	1000	1
10^{20}	1482	400	3000	1
10^{21}	500	600	3000	1
10^{20}	2110	450	500	20

Table 1. Simulation parameters, showing the adopted PBH mass and number, the size of the simulation box, the total number of runs, as well as the simulation time.

matter. However, due to our numerical setup with a spherical PBH halo, centered around the barycenter of the solar system, there is an additional acceleration for each solar system object due to the presence of dark matter,

$$\ddot{\mathbf{r}} = -\frac{4\pi G\rho_{\text{CDM}}}{3}\mathbf{r}. \quad (2)$$

Adding this term in the comparative simulation is necessary as we are interested in the perturbations induced by the PBHs and not in the numerical effect of the additional mass within the solar system. We want to mention that in this work we will focus on the perturbation of the magnitude of the vector,

$$\frac{|\delta\mathbf{r}|}{r}(t) = \frac{|(\tilde{\mathbf{r}}_{\text{earth}}(t) - \tilde{\mathbf{r}}_{\text{SSO}}(t)) - (\mathbf{r}_{\text{earth}}(t) - \mathbf{r}_{\text{SSO}}(t))|}{|\mathbf{r}_{\text{earth}}(t) - \mathbf{r}_{\text{SSO}}(t)|}, \quad (3)$$

which has the advantage of being strictly positive, whereas $\delta r/r$ typically oscillates between $-|\delta\mathbf{r}|/r$ and $|\delta\mathbf{r}|/r$ within one synodic orbital period of the SSO considered. While this quantity is more difficult to observe, it provides a reasonable estimate of the largest observable perturbation $\delta r/r$ per orbital period, as we show in Section 3.

To study the possibility of detecting or constraining PBHs we compare our simulation results to observational data. We can relate the magnitude of the induced perturbations to the measurement accuracy for solar system bodies. Currently available data for various solar system bodies allow the detection of perturbations as small as $\delta r/r \sim 10^{-11}$. At the moment, the most precise data are obtained for the Moon ($\mathcal{O}(1 \text{ mm})$), by lunar laser ranging (Battat et al. 2023; Colmenares et al. 2023), and for Mercury ($\mathcal{O}(0.7 \text{ m})$) and Mars ($\mathcal{O}(0.7 \text{ m})$) through various orbiters (Park et al. 2021). While the solar system objects have been monitored for a long time, precision data is only available for roughly the last two decades. In this work we will focus on the distance between Earth and Mars as it has been measured with high accuracy and is least susceptible to effects not considered in this work. These include most notably finite-size effects for the Moon and relativistic point-mass effects for Mercury (see Tran et al. (2023) for some estimates).

Finally, let us emphasize that our work does not aim to describe singular encounters with PBHs (for which we refer to Bertrand et al. (2023); Tran et al. (2023); Li et al. (2023)) but instead focuses on the cumulative effect of a whole halo of PBHs on the dynamics of the solar system.

3. RESULTS

Figure 1 shows the perturbations that are induced on the vector between Earth and Mars for $M_{\text{PBH}} \in [10^{18}, 10^{19}, 10^{20}, 10^{21}] \text{ g}$. Due to the random initial conditions of the PBHs for each run there is a significant variance in the value of $|\delta\mathbf{r}|/r$. The median value of the perturbations induced by a halo of PBHs is several orders of magnitude below the detection limit ($\delta r/r \sim 10^{-11}$) in each case and shows no significant dependence on the black hole mass M_{PBH} . The mean value of $|\delta\mathbf{r}|/r$ is higher than median and increases slightly with M_{PBH} . This can be understood analytically by the impulse approximation which is discussed in Section 4 and that is also displayed in Figure 1.

A statistical analysis of the perturbations is presented in Figure 2, where we show the probability distribution $p(|\delta\mathbf{r}|/r)$ of the perturbations of the Earth-Mars distance at $t=1 \text{ yr}$ in the left panel. The functions are obtained by a Gaussian kernel density estimate. Interestingly, there appears to exist no significant dependence on the PBH mass and for $M_{\text{PBH}} \geq 10^{19} \text{ g}$ we observe a power law tail with a slope of -2. Both results are interpreted by an analytical model in Section 4.1. The skewness of the distributions is the reason why we observe a larger mean value of the perturbations compared to the median, as mentioned above. For a subset of all simulations performed we also evaluate the distance of each SSO to the closest PBH. In the right panel of Figure 2 the perturbation strength $|\delta\mathbf{r}|/r$ at $t=1 \text{ yr}$ is plotted against the smallest distance b_{min} of Mars and Earth to a PBH within the simulation run. The dashed lines correspond to the analytical estimate of Equation 7.

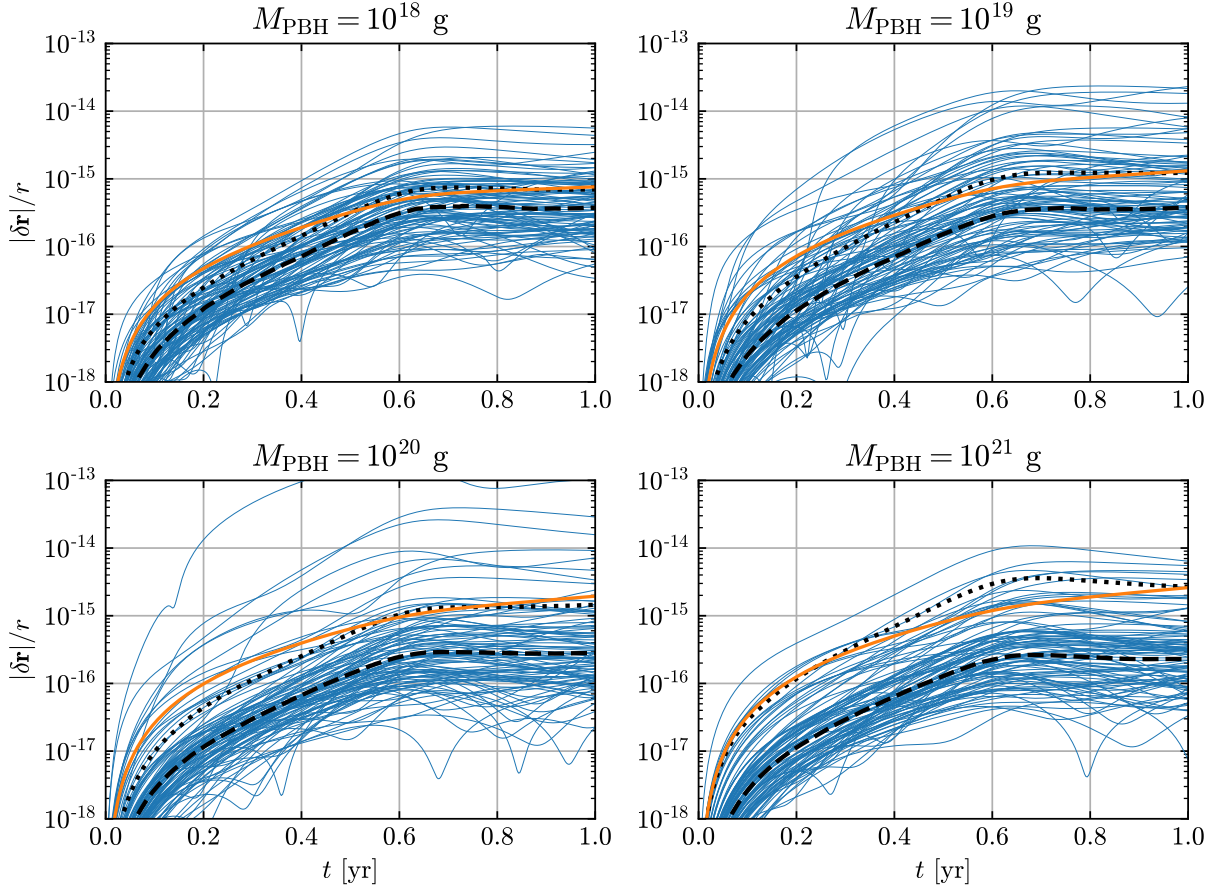


Figure 1. Perturbation of the vector between Earth and Mars, induced by PBHs for different values of their mass M_{PBH} . Each blue line corresponds to one simulation run. We only show 100 simulation runs in each case to make comparisons easier and improve readability. The black dashed/dotted line indicates the median/mean value obtained from all simulations. The analytical result of the impulse model for $b_{\text{max}} = 3b_{\text{min}}$ is shown as an orange line.

Finally, Figure 3 presents the results from 500 simulations performed over a longer time span of 20 years for $M_{\text{PBH}} = 10^{20}$ g. In the left panel we display the perturbation $|\delta\mathbf{r}|/r$ of the vector between Earth and Mars. A notable difference to Figure 1 is that the perturbations oscillate with a period of roughly two years which corresponds to the synodic orbital period of Mars and is thus simply a result of the change of r . We add an estimate for a 3σ detection limit by assuming that $\sigma_r \approx 70$ cm for the Earth-Mars distance (Park et al. 2021). Out of all 500 simulation runs only 4 exceed this limit at least once within 20 yrs, implying a $\sim 1\%$ chance of detection with a confidence level of 3σ .

In the right panel of Figure 3 we show the mean perturbation strength $|\delta\mathbf{r}|/r$ of all simulation runs for the vector between Earth and each planet. Notably, $|\delta\mathbf{r}|/r$ is very similar for the inner planets while it decreases for the outer planets as the distance to the Earth gets larger. This can be understood by the impulse model (see Section 4.1) which predicts two different regimes, depending on whether the typical impact parameter of the PBH b is much smaller or much larger than the distance r between the Earth and the other SSO. Since $b_{\text{min}} \approx 3.4$ AU for our parameters (from Equation 9) one has $b_{\text{min}} > r$ for the inner planets and $b_{\text{min}} < r$ for the outer planets.

In the results presented in this study, we analyse the perturbation of the vector $|\delta\mathbf{r}|$ between the Earth and other SSOs. However, only the perturbation of the distance δr can be observed with high accuracy. We argue that this should not affect our results as δr typically oscillates between $-|\delta\mathbf{r}|$ and $|\delta\mathbf{r}|$ and thus our results can be regarded as an upper bound of the observable perturbation since $|\delta r| \leq |\delta\mathbf{r}|$ by definition. To test this statement we compare the values of δr and $\delta\mathbf{r}$ for the vector between Earth and Mars. We use the data from the last synodic orbital period from the 500 simulations performed over a timespan of $t = 20$ yr. We find that 87% of the simulations reach $|\delta r| > |\delta\mathbf{r}|/2$ at least once and 72% of the simulations reach $|\delta r| > |\delta\mathbf{r}|/2$ during at least 75% of the respective timespan. In addition,

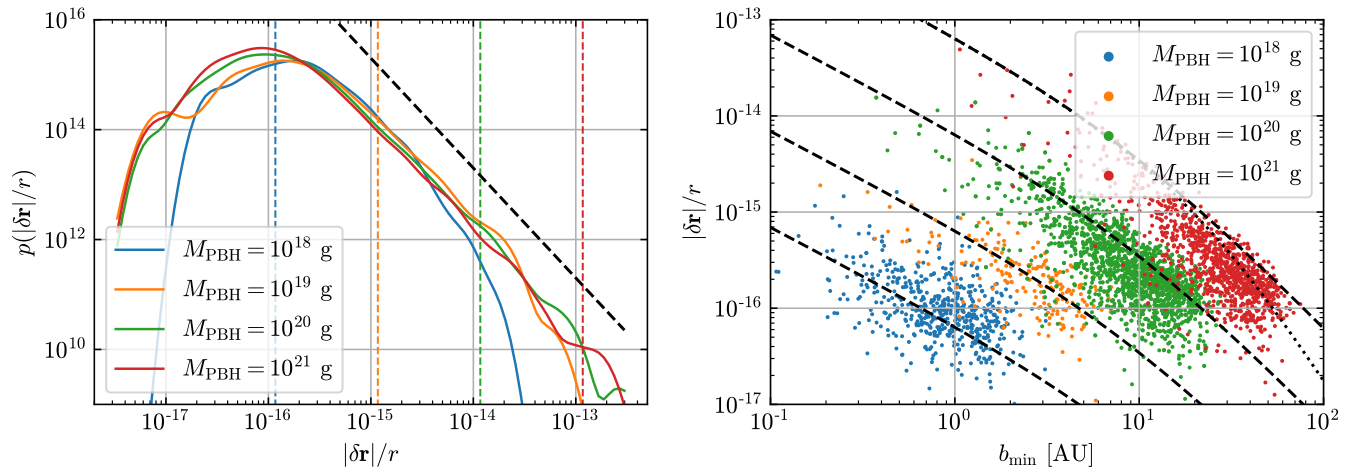


Figure 2. *Left:* Probability distribution function of the perturbation $|\delta\mathbf{r}|/r$ of the Earth-Mars vector, evaluated at $t = 1.0$ yr for different values of the PBH mass M_{PBH} . The black dashed line indicates a power law with slope of -2. Vertical, dashed lines indicate the critical perturbation $(|\delta\mathbf{r}|/r)_{\text{crit}}$, that is defined in Equation 11, for each value of M_{PBH} . *Right:* Perturbation strength $|\delta\mathbf{r}|/r$ of the Earth-Mars vector, evaluated at $t = 1.0$ yr vs. the minimum impact parameter b_{min} observed within the simulation period. The black, dashed lines correspond to Equation 7. The dotted line for $M_{\text{PBH}} = 10^{21}$ g takes into account the finite distance travelled by the PBHs within the simulation time and is explained in Section 4.4.

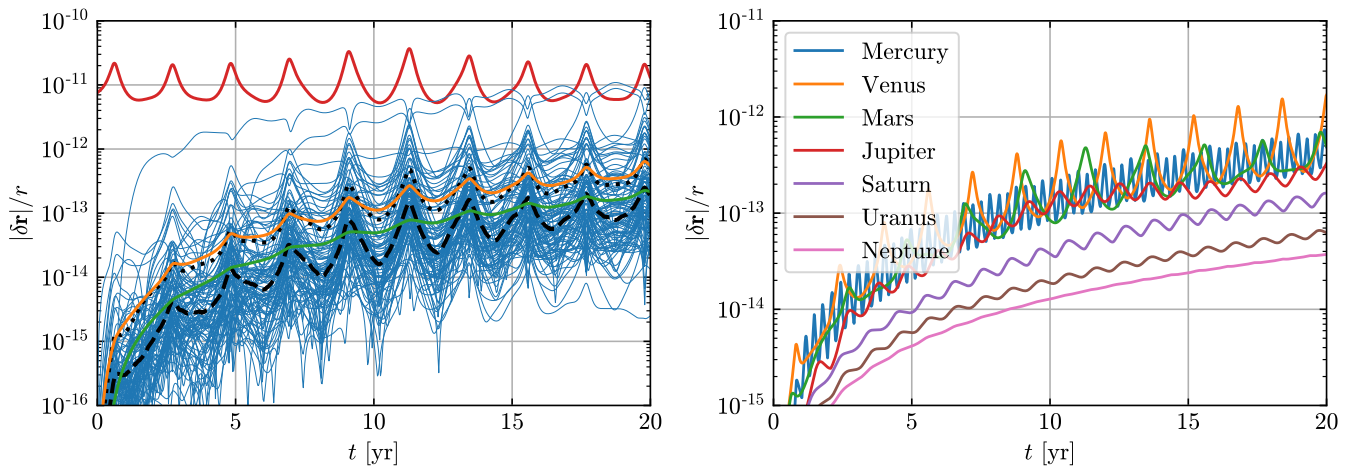


Figure 3. *Left:* Perturbation of the vector between Earth and Mars induced by PBHs for $M_{\text{PBH}} = 10^{20}$ g as a function of time. Each blue line corresponds to one simulation run. We only show 100 simulation runs to improve readability. The black dashed/dotted line indicates the median/mean value obtained from all 500 simulations. The analytical result of the impulse model is displayed as an orange line. The green line shows a model for the median perturbation strength, given by Equation 14. The red line is an estimate of the 3σ observational detection limit. *Right:* Mean perturbation strength $|\delta\mathbf{r}|/r$ as a function of time for the vector between Earth and each planet.

50% of the simulations reach $|\delta r| > 0.9|\delta\mathbf{r}|$ at least once within the orbital period. This justifies our approach of studying the perturbation of the vector $\delta\mathbf{r}$ as a good approximation of the largest observable perturbation of the distance δr .

4. DISCUSSION

4.1. Impulse Model

The results obtained from our simulations show that the perturbations induced by a halo of PBHs grow over time, to a median value of $|\delta\mathbf{r}|/r \sim 10^{-13}$ within 20 years. To provide some analytical understanding of our results we make use of the impulse approximation (Binney & Tremaine 2008), which assumes that a PBH moves in a straight line with an impact parameter (distance of closest approach) b . Then the velocity change induced on a SSO in the direction

perpendicular to the motion of the PBH is

$$\Delta v \approx \int dt \frac{GM_{\text{PBH}}b}{(b^2 + (v_{\text{PBH}}t)^2)^{3/2}} = \frac{2GM_{\text{PBH}}}{bv_{\text{PBH}}}. \quad (4)$$

In the following, we also assume that all PBHs move perpendicular to the ecliptic plane which is a first order approximation that greatly simplifies our calculations and is also motivated by our initial conditions (see Section 2). This implies that the point of closest approach is identical for all bodies in the solar system and will be reached when the PBH crosses the ecliptic plane. Let us first assume that the impact parameter b is much larger than the distance r between Earth and another SSO (in our case Mars). In this case, the Earth and the other object will be perturbed by the same amount Δv but in slightly different directions, with an angle between $\Delta \mathbf{v}_{\text{earth}}$ and $\Delta \mathbf{v}_{\text{SSO}}$ of $\alpha \approx r/b$. This means

$$|\delta \mathbf{r}| = |\Delta \mathbf{v}_{\text{earth}} - \Delta \mathbf{v}_{\text{SSO}}|t \approx \frac{\Delta v r t}{b} \approx \frac{2GM_{\text{PBH}} r t}{b^2 v_{\text{PBH}}}. \quad (5)$$

If, on the other hand, $b \ll r$, we only need to consider the velocity change of the body closest to the PBH,

$$|\delta \mathbf{r}| = |\Delta \mathbf{v}_{\text{earth}} - \Delta \mathbf{v}_{\text{SSO}}|t \approx \Delta v t = \frac{2GM_{\text{PBH}} t}{bv_{\text{PBH}}}. \quad (6)$$

In the intermediate case, the perturbation strength depends on the specific geometry. Numerically, by averaging over all possible geometries for a fixed b , we find that

$$\frac{|\delta \mathbf{r}|}{r} \approx \frac{2GM_{\text{PBH}} t}{(br + b^2)v_{\text{PBH}}} \quad (7)$$

provides a reasonable fit to the numerical data, with a maximum deviation of a factor of 2.2 at $b = r/2$. For the mean perturbation strength $\langle |\delta \mathbf{r}|/r \rangle$ that we discuss below the difference is at most 20%. The numerical result is discussed further in Section A in the Appendix.

So far, we have considered the perturbation from a single encounter with a PBH. For a DM halo composed of PBHs the rate of encounters in the solar system will be $\Gamma = (\sigma/m)\rho v = (\pi b^2/M_{\text{PBH}})\rho_{\text{CDM}}v_{\text{PBH}}$. This means that the number of scattering events per interval of b is $dN/db = (2\pi b/M_{\text{PBH}})\rho_{\text{CDM}}v_{\text{PBH}}t$. From this we can obtain the perturbation strength,

$$\left\langle \frac{|\delta \mathbf{r}|}{r} \right\rangle \approx \int_0^{b_{\text{max}}} db \frac{dN}{db} \frac{2GM_{\text{PBH}} t}{(br + b^2)v_{\text{PBH}}} = 4\pi G \rho_{\text{CDM}} t^2 \log(1 + b_{\text{max}}/r). \quad (8)$$

In principle b_{max} can be as large as the boxsize R_{box} of our simulation. However, with increasing distance the number of PBH encounters grows until they will no longer cause individual perturbations but rather behave as a spherically symmetric mass distribution. Let us define b_{min} as the minimum impact parameter for which we expect one scattering event within the time t :

$$b_{\text{min}} = \sqrt{\frac{M_{\text{PBH}}}{\pi \rho_{\text{CDM}} v_{\text{CDM}} t}}. \quad (9)$$

One expects N^2 encounters with an impact parameter $b = Nb_{\text{min}}$ within the same time period. However, as N becomes large, these perturbations will begin to cancel each other out due to the random orientation of $\delta \mathbf{v}$. As can be seen in Figure 1 and Figure 3 (left panel) the choice $b_{\text{max}} = 3b_{\text{min}}$ provides a very good fit to the actual mean perturbation. Due to the logarithmic dependence on b_{max} the precise factor is not of great importance in any case.

The fact that the perturbations are dominated by the closest encounter is also demonstrated in the right panel of Figure 2, where we plot the perturbation strength $|\delta \mathbf{r}|/r$ at $t = 1$ yr against the smallest impact parameter within the simulation run. The observed values agree reasonably well with Equation 7 that is displayed as dashed lines. Note that here we have assumed a singular encounter with a PBH that moves perpendicular to the ecliptic plane. Therefore, some deviation from the analytical estimates is expected in the more complex simulation environment. In addition, the approximation of infinite integration boundaries in Equation 4 breaks down for large PBH masses which explains part of the offset observed for $M_{\text{PBH}} = 10^{21}$ g. This will be discussed in more detail in Section 4.3.

Equation 8 provides a simple explanation for the observed weak dependence of the perturbation strength $|\delta \mathbf{r}|/r$ on the black hole mass as it predicts only a logarithmic dependence as long as $b_{\text{max}} \gg r$. The underlying reason is that the strength of the gravitational force ($\sim M_{\text{PBH}}$) is counteracted by the decrease in the scattering rate ($\sim 1/M_{\text{PBH}}$). This

means, our simulation results should have some validity beyond the mass range considered here. However, if PBHs are sufficiently light (or t sufficiently long) then one could have $b_{\max} \ll r$ (assuming again that $b_{\max} \sim \mathcal{O}(b_{\min})$ as we argued above) and thus $|\delta\mathbf{r}|/r \sim \log(1 + b_{\max}/r) \approx b_{\max}/r \sim \sqrt{M_{\text{PBH}}}$. For $t = 1$ yr one has $b_{\min} = r$ for $M_{\text{PBH}} \sim 10^{18}$ g. Indeed, in our simulation results we notice a decreasing strength of the mean amplitude of the perturbations as M_{PBH} decreases (compare the dotted black lines across the four panels in Figure 1). In addition, this explains the declining strength of $|\delta\mathbf{r}|/r$ for the outer planets in the right panel of Figure 3 as one has $b_{\max} < r$ there. Finally, we want to emphasize that the decreasing strength of the perturbations at low PBH masses provides consistency as they should disappear as $M_{\text{PBH}} \rightarrow 0$ and one obtains a smooth DM component.

4.2. Statistics of the perturbations

The impulse model derived in the previous Section allows us to interpret the results obtained for the probability distribution $p(|\delta\mathbf{r}|/r)$. Notably, a power law tail with a slope of -2 is observed for $M_{\text{PBH}} \geq 10^{19}$ g (see the left panel of Figure 2). The homogeneous distribution of PBHs implies that the distribution of impact parameters is given by $p(b) \sim b$. If we assume $b \gg r$, then we can use Equation 5 to obtain

$$p(|\delta\mathbf{r}|/r) = p(b) \left| \frac{db}{d|\delta\mathbf{r}|/r} \right| \sim (|\delta\mathbf{r}|/r)^{-2}, \quad (10)$$

which explains the observed power law. To understand the validity of $b \gg r$ let us define the critical perturbation $|\delta\mathbf{r}|/r_{\text{crit}}$ as the value obtained from Equation 7 for $b = r$,

$$\left(\frac{|\delta\mathbf{r}|}{r} \right)_{\text{crit}} = \frac{GM_{\text{PBH}}\Delta t}{r^2 v_{\text{PBH}}}. \quad (11)$$

The values of $|\delta\mathbf{r}|/r_{\text{crit}}$ are displayed as vertical lines in the left panel of Figure 2. For $|\delta\mathbf{r}|/r > |\delta\mathbf{r}|/r_{\text{crit}}$ the approximation $b \gg r$ breaks down. For $M_{\text{PBH}} \in [10^{20}, 10^{21}]$ g most of the observed perturbations are below the critical value and indeed $p(|\delta\mathbf{r}|/r)$ follows a power law with a slope of -2 to good agreement. For $M_{\text{PBH}} = 10^{18}$ g, most of the perturbations are far above the critical value and our approximation breaks down, which explains the observed deviation from the expected power law. At $M_{\text{PBH}} = 10^{19}$ we observe a power law with a slope of -2 for perturbations up to $|\delta\mathbf{r}|/r \sim 10|\delta\mathbf{r}|/r_{\text{crit}}$ which suggests that Equation 10 is valid up to that point. We cannot make strong statements for the behaviour of the distribution function beyond this, based on our simulation data, as the occurrence of such perturbations is too rare and we are thus limited by the number of simulations that we have performed. If we trust the analytical model from Section 4.1 for $b \ll r$ then, using Equation 6, one would expect $p(|\delta\mathbf{r}|/r) \sim (|\delta\mathbf{r}|)^{-3}$ in this regime.

4.3. Extrapolating our results

Our simulations help us to investigate perturbations induced by PBHs for a certain range of masses M_{PBH} and timescales t . We find that the dependence on the mass of the PBH is only logarithmic as long as $b_{\max} \gg r$ and, for the parameters that we studied, the results are well described by the impulse model, discussed in Section 4.1. Therefore one can attempt to use our analytical model to extend the study to longer timescales and to wider range of PBH masses that we could not investigate so far due to the computational expense of running a large number of additional simulations. However, it is necessary to make one modification to the impulse model. The reason is that for large PBH masses and small timescales one can no longer take the integration boundaries in Equation 4 to infinity as the timescale of a fly-by of a black hole will take longer than the observation time t . If one takes into account the finite distance travelled by the PBH one obtains:

$$\Delta v \approx \int_{-t/2}^{t/2} dt' \frac{GM_{\text{PBH}}b}{(b^2 + (v_{\text{PBH}}t')^2)^{3/2}} = \frac{2GM_{\text{PBH}}}{bv_{\text{PBH}}} \frac{\frac{v_{\text{PBH}}t}{2b}}{\sqrt{1 + \left(\frac{v_{\text{PBH}}t}{2b}\right)^2}} \quad (12)$$

From this, one obtains the explicit expression for the perturbation strength,

$$\frac{|\delta\mathbf{r}|}{r} \approx \frac{2GM_{\text{PBH}}t}{(rb + b^2)v_{\text{PBH}}} \frac{\frac{v_{\text{PBH}}t}{2b}}{\sqrt{1 + \left(\frac{v_{\text{PBH}}t}{2b}\right)^2}}. \quad (13)$$

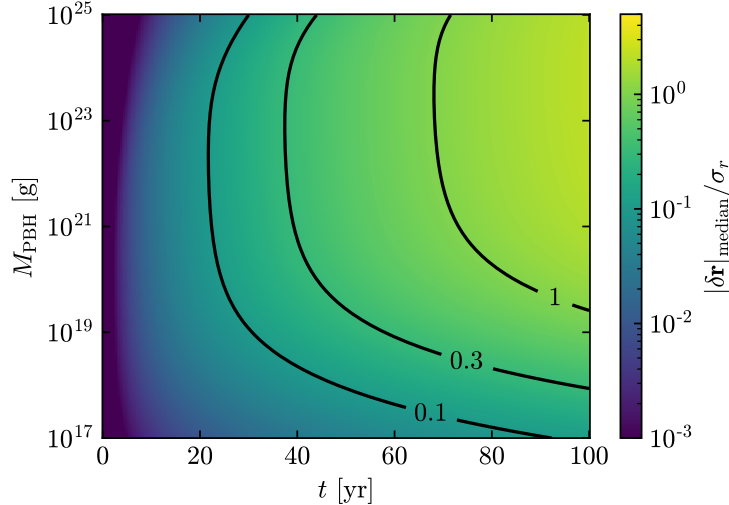


Figure 4. Estimated median signal-to-noise ratio $|\delta\mathbf{r}|_{\text{median}}/\sigma_r$ for the observation of the Earth-Mars distance as a function of the PBH mass and the timescale, assuming $\sigma_r = 70$ cm. Contour levels are drawn for several values of the SNR. The results are obtained using the impulse model, presented in Section 4.1 and refined in Section 4.3.

For $v_{\text{PBH}}t \gg b$ this reduces to the expression in Equation 7, as expected. However, for large impact parameters (i.e. large PBH masses) or on small timescales one obtains $|\delta\mathbf{r}|/r \sim b^{-3}$. To demonstrate the effect of this modification we show this improved model as a dotted line for $M_{\text{PBH}} = 10^{21}$ g in the right panel of Figure 2. Taking into account the finite travel distance in Equation 12 leads to better agreement with the simulation data. We make use of this improved model in the next Section, where we investigate the detectability of the perturbations induced by PBHs

4.4. Prospects for detecting PBHs

The quantity of interest for detecting PBHs is the ratio between the perturbations $|\delta\mathbf{r}|$ that they induce and the observational residual σ_r in the distance between Earth and a given SSO. In Section 4.2 we found that the distribution of perturbations $p(|\delta\mathbf{r}|/r)$ is highly skewed. This means that the mean perturbation strength is not a good measure for detectability as the likelihood to observe it can be low. Of the 500 simulation that were performed for $t = 20$ yr, 113 end up with a perturbation strength $|\delta\mathbf{r}|/r$ which is larger than the mean $\langle|\delta\mathbf{r}|/r\rangle$, a fraction of $\sim 27\%$. Therefore it is more useful to compare the median perturbation strength to the observational residual. If $|\delta\mathbf{r}|_{\text{median}} > \alpha\sigma_r$ then there is 50% chance for an observation with a signal-to-noise ration of α . In Section 4.1 we have derived the impulse model to describe the mean perturbation strength. To a good approximation, the median perturbation strength can be estimated by setting the minimum impact parameter to b_{min} (Equation 9) when performing the integration over b ,

$$\left(\frac{|\delta\mathbf{r}|}{r}\right)_{\text{median}} \approx \int_{b_{\text{min}}}^{b_{\text{max}}} db \frac{dN}{db} \frac{2GM_{\text{PBH}}t}{(rb + b^2)v_{\text{PBH}}} \frac{\frac{v_{\text{PBH}}t}{2b}}{\sqrt{1 + \left(\frac{v_{\text{PBH}}t}{2b}\right)^2}}. \quad (14)$$

The reason is that the median perturbation will be dominated by the smallest 'typical' impact parameter b_{min} , whereas the mean takes into account smaller values of b that can occur rarely and is thus skewed to larger values. We demonstrate the validity of this assumption in the left panel of Figure 3 where we show the result from Equation 14 as the green line, which agrees well with the median from the simulation data (black, dashed line).

Figure 4 presents the signal-to-noise ratio (SNR) $|\delta\mathbf{r}|_{\text{median}}/\sigma_r$ for the Earth-Mars distance using Equation 8 and $b_{\text{max}} = 3b_{\text{min}}$, although the results are not very sensitive to the precise value of b_{max} as discussed in Section 4.1. A value of $\sigma_r = 70$ cm is assumed for the residual of the Earth-Mars distance (Park et al. 2021). Note that the dependence of $|\delta\mathbf{r}|_{\text{median}}$ on M_{PBH} is only logarithmic for $M_{\text{PBH}} \in [10^{19}, 10^{23}]$ g. At low masses, when $b_{\text{max}} \ll r$, one has $|\delta\mathbf{r}|_{\text{median}} \sim \sqrt{M_{\text{PBH}}}$ and at high masses $|\delta\mathbf{r}|_{\text{median}} \sim 1/\sqrt{M_{\text{PBH}}}$.

As a conservative estimate, we regard the perturbations induced by the halo of PBHs as a random signal and thus a SNR greater than 1 is required for detection. We find that a significant detection ($|\delta\mathbf{r}|_{\text{median}}/\sigma_r \geq 3$) cannot be reached with 100 years of observational data. If the uncertainty in the distance σ_r decreases by a factor of 30, then only

around 20-30 years of data are required to detect PBHs with a mass $M_{\text{PBH}} \in [10^{19}, 10^{24}]$ g with 3σ confidence (this corresponds to the 0.1 contour in Figure 4). Note that $|\delta\mathbf{r}| \sim \rho_{\text{CDM}}$ and hence the detection window becomes larger if the local dark matter density is greater than the assumed value of $\rho_{\text{CDM}} = 7 \times 10^{-25}$ g cm $^{-3}$. We want to emphasize that the results presented in Figure 4 are based on the analytical impulse model and for particular parameters one should perform a set of numerical simulations to obtain more accurate results. It would also be interesting to study the probability of detection for a given SNR as a function of M_{PBH} and t . However, this requires a better understanding of $p(|\delta\mathbf{r}|/r)$ that is beyond the scope of this work.

So far, we have treated the perturbations as a random signal and thus required a $\text{SNR} > 1$ for detection. However, the perturbations induced by the encounters of PBHs likely have certain characteristics that can be exploited to make predictions of the expected signal $\delta r(t)$. In that case, one can attempt to use template matching techniques in order to detect perturbations with an amplitude well below the noise level σ_r . This was studied by [Tran et al. \(2023\)](#) who found that there will be a sizeable number of detectable events if the extraction of signals with a SNR well below 10^{-2} is achieved. A possible caveat regarding the detection of PBHs are potential degeneracies between the perturbations induced by the PBHs and other gravitational effects in the solar system. Accurate models of solar system ephemerides are obtained by iterating over a large number of free parameters, including the physical parameters of all SSOs. To assess the prospects of detecting PBHs one has to study the degree of degeneracy between the perturbations that they induce and a change in one of the other parameters of these models.

4.5. Poissonian Fluctuations

In our work, we analyze at the cumulative gravitational effect of PBHs on the orbits of solar system objects. We find that the perturbations induced by the black holes are dominated by the closest encounter (see Section 4.1). This is in contrast to the work by [Loeb \(2024\)](#) which studies the influence of Poissonian fluctuations in the PBH density. If the dark matter is composed of asteroid-mass black holes then their number within the solar system can undergo sizeable Poisson fluctuations. [Loeb \(2024\)](#) considered the rate of change in the total mass of PBHs within a distance R from the Sun, given by

$$\delta\dot{M} = 1.9 \times 10^{-13} \left(\frac{M_{\text{PBH}}}{10^{20} \text{ g}} \right)^{1/2} \left(\frac{R}{50 \text{ AU}} \right)^{1/2} M_{\odot} \text{ yr}^{-1}. \quad (15)$$

In his work it is then assumed that such fluctuations would induce similar effects as if a point mass in the center of the solar system would change its mass with the same rate, effectively changing the solar mass by a small amount. For $R = 50$ AU and $M_{\text{PBH}} \in [6 \times 10^{18}, 10^{22}]$ g, this would lead to a rate $\delta\dot{M}$ larger than the constraint on \dot{M}_{sol} by [Pitjeva et al. \(2021\)](#) and thus he concluded that PBHs in this mass range cannot make up the entire dark matter.

It is important to note that these Poissonian fluctuations can only occur if there is at least one PBH in the volume of interest. For Mars one requires $M_{\text{PBH}} \lesssim 3 \times 10^{16}$ g to have at least one PBH inside its orbit. At these low PBH masses the fluctuations that follow from Equation 15 are well below the observational constraint from [Pitjeva et al. \(2021\)](#) and thus cannot be used to rule out PBHs as dark matter. For the outer planets, the fluctuations from Equation 15 can exceed the constraint on \dot{M}_{sol} , as e.g. for Neptune one requires $M \lesssim 3 \times 10^{20}$ g which implies a value of $\delta\dot{M} < 2.5 \times 10^{-13} M_{\odot} \text{ yr}^{-1}$. However, it is not justified to apply the constraint by [Pitjeva et al. \(2021\)](#) for the outer planets in isolation as it was derived from the entire set of solar system data, assuming no dependence of \dot{M}_{sol} on r , and is dominated by the effect of fluctuations on the inner planets. On the one hand, this is because the observational data of the inner planets currently has the highest accuracy. On the other hand, a change in the solar mass has a much stronger effect on the inner planets compared to the outer ones, as the additional force from the change in the solar mass will be proportional to $\delta\dot{M}/r^2$. In essence, an observational constraint on \dot{M}_{sol} at the orbital distance of Neptune would be orders of magnitude weaker than the limit which [Loeb \(2024\)](#) is using. Note that similar remarks were already made by [Cline \(2024\)](#).

For the reasons stated above, one cannot rule out PBHs based on the Poisson fluctuation in their number density. Nevertheless, it remains of interest to compare the effects of these fluctuations to those from individual encounters. To investigate this, we perform a simulation where, at each timestep and for each planet, we count the number of PBHs $N_{\text{PBH}}(t, r_i)$ within the orbital distance r_i of the planet i to the Sun. We then set the solar mass for each planet to $M_{\text{sol},i}(t) = M_{\odot} + M_{\text{PBH}} N_{\text{PBH}}(t, r_i)$. The PBHs do not exert any gravitational force on the solar system bodies in this simulation, acting only through the fluctuations of the solar mass. One has to have at least one PBH inside the orbit of a planet to observe any fluctuations. For Mercury this implies $M_{\text{PBH}} \lesssim 4 \times 10^{14}$ g which would lead to a computationally infeasible number of PBHs within the entire solar system. We therefore study the inner and

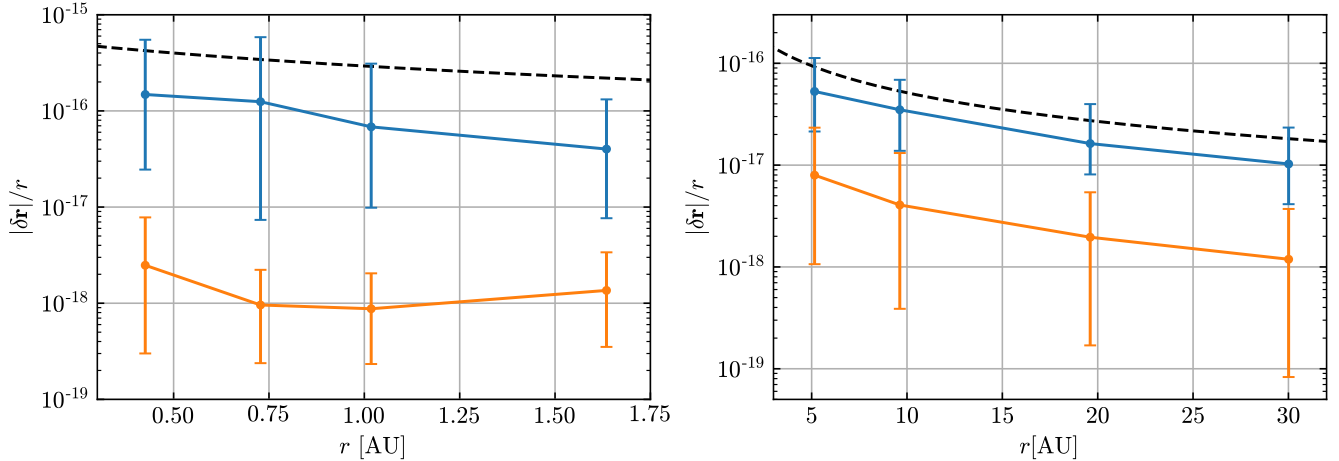


Figure 5. Perturbation of the vector between the Sun and the planets in the solar system. The left panel shows the results for a simulation of the inner solar system with $M_{\text{PBH}} = 3 \times 10^{13}$ g at $t = 3$ yr. In the right panel, we present the results for the outer solar system with $M_{\text{PBH}} = 10^{17}$ g at $t = 1$ yr. Each data point corresponds to the median perturbation of 100 simulation runs. The errorbars indicate the range that includes 90% of the simulation results. The blue points correspond to our usual simulation setup. In orange, we show the results of simulations where the solar mass is changing according to the Poisson fluctuations of PBHs $\delta\dot{M}$, as explained in Section 4.5.

outer planets in two separate simulations. For the simulation containing the inner planets and the Earth’s moon we choose $M_{\text{PBH}} = 3 \times 10^{13}$ g and $L_{\text{box}} = 10$ AU, whereas we take $M_{\text{PBH}} = 10^{17}$ g and $L_{\text{box}} = 150$ AU for the outer planets. This means that there will be on average $\langle N_{\text{PBH}} \rangle \in [13, 120, 347, 858]$ PBHs inside the orbits of Mercury, Venus, Earth, and Mars. For Jupiter, Saturn, Uranus, and Neptune there will be $\langle N_{\text{PBH}} \rangle \in [12, 89, 737, 2622]$ PBHs inside their orbits. In Figure 5 we display the perturbations of the vector between the Sun and each planet. The left panel shows the results for the inner solar system at $t = 3$ yr, whereas the simulation for the outer planets are shown in the right panel for $t = 1$ yr. Blue points indicate the median value for simulations where we include the gravity of the PBHs, whereas the orange points show the results for the simulations with a fluctuating solar mass. The perturbations induced by PBHs on the orbit of the planets are roughly an order of magnitude larger compared to the effect of Poisson fluctuations of the solar mass. Based on these results alone, one can not distinguish whether the disagreement is because the Poisson fluctuations are a small contribution to the total effect of PBHs in the solar system or because one cannot treat the Poisson fluctuations of the PBH number density as a change in the solar mass. However, the analytical model introduced in Section 4.1 suggests that the perturbations induced by PBHs can be predicted with good accuracy by taking into account the closest encounters. We display the model for the median perturbation strength from Equation 14 as a dashed line in Figure 5 and it shows reasonable agreement for $b_{\text{max}} = 3b_{\text{min}}$. This suggests that Poisson fluctuations likely play only a minor role in the overall gravitational effect of PBHs on the solar system bodies.

4.6. Limitations of this work

With our model one is able to make general statements about the strength and evolution of perturbations induced by PBHs and to study whether they are in conflict with current data. However, in order to detect individual PBHs one needs a precise model for solar system ephemerides that includes more solar system bodies and treatment of finite-size effects, radiation pressure, relativistic corrections, and other effects that we have neglected. It is crucial to study the possible degeneracy between the mentioned effects and the perturbations induced by the PBHs. A combination of such a model, together with a sophisticated analysis of solar system ephemerides could be a viable pathway to the detection of asteroid-mass PBHs.

For the halo of PBHs, we have assumed a monochromatic mass function for simplicity. In reality, PBHs are likely to form with an extended mass distribution. While one can easily expand our analysis for a distribution of PBH masses, it is not straightforward to connect this distribution to the initial PBH mass function at formation in the early Universe. The main reason for this is that one has to deal with migration effects, where the heavier black holes sink towards the

center of the halo while the lighter ones move outwards. In general, we do not expect that an extended mass function would change the perturbations of PBHs in a drastic way as we found little mass dependence in our results.

A more sizeable impact on our results could be expected if PBHs are clustered (see Section II of Carr et al. (2024) and references therein). If the size of such a cluster is small compared to the impact parameter, then it will simply act as a much heavier black hole. However, if the size of such a cluster is comparable to the solar system then our results could change in a non-trivial way. In addition, the degree of clustering might be dependent on the black hole mass in which case an extended mass function could have a sizeable impact on the result. Therefore, it would be worthwhile to study this aspect in a future work.

5. SUMMARY

In this work, we perform numerical simulations of the solar system, embedded in a DM halo of PBHs. The simulation results are used to quantify the perturbations induced by the PBHs on the distances between the Earth and other planets. First, it is demonstrated that the strength of the perturbations depends only weakly on the PBH mass in the range $10^{18} \text{ g} < M_{\text{PBH}} < 10^{21} \text{ g}$. The physical reason for this is the fact that the strength of the gravitational force ($\sim M_{\text{PBH}}$) is balanced by the scattering rate ($\sim 1/M_{\text{PBH}}$). We then show for $M_{\text{PBH}} = 10^{20} \text{ g}$ that after a time span of 20 years the perturbations are still more than an order of magnitude below the current precision of observational data for the Earth-Mars distance, which has been available for a similar time period. Therefore, PBHs cannot be directly constrained based on solar system ephemerides, challenging the results of recent work.

Our results are interpreted by a simple analytical model that provides an independent test of the accuracy of our simulations. In addition, it enables us to extrapolate to longer timescales and to a larger range of PBH masses. We find that the precision of solar system ephemerides has to increase by more than an order of magnitude for the effect of the PBH halo to become noticeable within a decade of observation. In order to reliably detect PBHs it is necessary to employ accurate models of solar system ephemerides that include finite-size effects, relativistic corrections and other effects that were neglected in this work.

We thank Avi Loeb whose work has inspired us to pursue this project. We also would like to thank Chris McKee and Florian Kühnel for fruitful discussions and helpful comments. This research was supported by the Excellence Cluster ORIGINS which is funded by the Deutsche Forschungsgemeinschaft (DFG, German Research Foundation) under Germany's Excellence Strategy - EXC-2094 - 390783311.

Software: Julia (Bezanson et al. 2017), Matplotlib (Hunter 2007)

APPENDIX

A. RELATION BETWEEN THE PERTURBATION STRENGTH AND THE IMPACT PARAMETER

In Section 4.1 we derived expressions for the relation between the perturbation strength $|\delta\mathbf{r}|/r$ and the impact parameter b in the limit $b \gg r$ (Equation 5) and for $b \ll r$ (Equation 6). In the intermediate case $b \sim r$ the result will strongly depend on the precise geometry of the encounter. To investigate this effect we uniformly sample 10^7 PBH positions in a plane around two SSOs that are separated by distance $r = 1$. For each PBH position we determine the minimum of the distance to both bodies b and the perturbation strength $|\delta\mathbf{r}|/r$. Figure 6 shows the range of values obtained for $|\delta\mathbf{r}|$ for each value of b as the shaded area and the mean values as points. We have set $2GM_{\text{PBH}}\Delta t/v_{\text{PBH}} = r = 1$ as we only care about the functional dependence on b . The analytical relation (Equation 7) that we use in this work is shown as the orange line and agrees well with the numerical data. The strongest deviation is a factor of 2.2 for $b \approx r/2$. If we integrate over the numerical relation then we find a deviation of at most 20%. This justifies using Equation 7 to describe the simulation results.

REFERENCES

- Abbott, B. P., Abbott, R., Abbott, T. D., et al. 2016, PhRvL, 116, 061102, doi: 10.1103/PhysRevLett.116.061102
- Adams, A. W., & Bloom, J. S. 2004, arXiv e-prints, astro, doi: 10.48550/arXiv.astro-ph/0405266

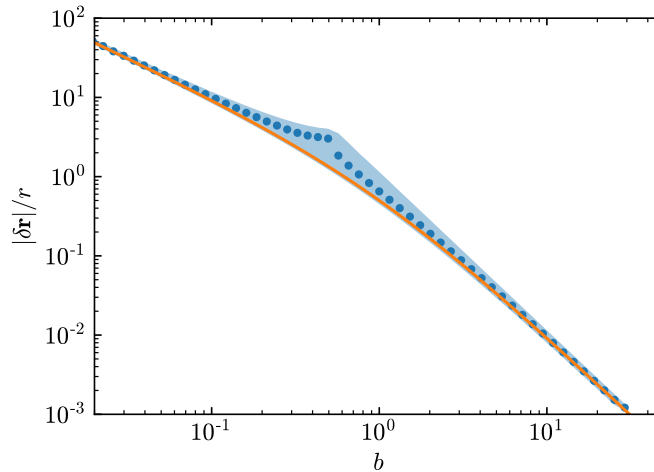


Figure 6. Strength of the perturbation $|\delta\mathbf{r}|/r$ induced by a fly-by of a PBH as a function of the impact parameter b . The shaded area displays the range of values for all possible geometries. The blue dots indicate the mean value averaged over all configurations. The analytical relation from Equation 7 is shown as the orange line.

- Alexandre, A., Dvali, G., & Koutsangelas, E. 2024, *PhRvD*, 110, 036004, doi: [10.1103/PhysRevD.110.036004](https://doi.org/10.1103/PhysRevD.110.036004)
- Battat, J. B. R., Adelberger, E., Colmenares, N. R., et al. 2023, *PASP*, 135, 104504, doi: [10.1088/1538-3873/aceb2f](https://doi.org/10.1088/1538-3873/aceb2f)
- Bertrand, B., Cuadrat-Grzybowski, M., Defraigne, P., Van Camp, M., & Clesse, S. 2023, arXiv e-prints, arXiv:2312.14520, doi: [10.48550/arXiv.2312.14520](https://doi.org/10.48550/arXiv.2312.14520)
- Bezanson, J., Edelman, A., Karpinski, S., & Shah, V. B. 2017, *SIAM Review*, 59, 65, doi: [10.1137/141000671](https://doi.org/10.1137/141000671)
- Binney, J., & Tremaine, S. 2008, *Galactic Dynamics: Second Edition*
- Caplan, M. E., Johnston, J., & Santarelli, A. D. 2023, *MNRAS*, 524, 1927, doi: [10.1093/mnras/stad1846](https://doi.org/10.1093/mnras/stad1846)
- Carr, B., Kohri, K., Sendouda, Y., & Yokoyama, J. 2021, *Reports on Progress in Physics*, 84, 116902, doi: [10.1088/1361-6633/ac1e31](https://doi.org/10.1088/1361-6633/ac1e31)
- Carr, B. J., Clesse, S., García-Bellido, J., Hawkins, M. R. S., & Kühnel, F. 2024, *PhR*, 1054, 1, doi: [10.1016/j.physrep.2023.11.005](https://doi.org/10.1016/j.physrep.2023.11.005)
- Carr, B. J., & Green, A. M. 2024, arXiv e-prints, arXiv:2406.05736, doi: [10.48550/arXiv.2406.05736](https://doi.org/10.48550/arXiv.2406.05736)
- Cline, J. M. 2024, arXiv e-prints, arXiv:2409.01993, doi: [10.48550/arXiv.2409.01993](https://doi.org/10.48550/arXiv.2409.01993)
- Colmenares, N. R., Battat, J. B. R., Gonzales, D. P., Murphy, T. W., & Sabhlok, S. 2023, *PASP*, 135, 104503, doi: [10.1088/1538-3873/acf787](https://doi.org/10.1088/1538-3873/acf787)
- Freese, K., Lisanti, M., & Savage, C. 2013, *Reviews of Modern Physics*, 85, 1561, doi: [10.1103/RevModPhys.85.1561](https://doi.org/10.1103/RevModPhys.85.1561)
- Hunter, J. D. 2007, *Computing in Science & Engineering*, 9, 90, doi: [10.1109/MCSE.2007.55](https://doi.org/10.1109/MCSE.2007.55)
- Li, Y.-L., Huang, G.-Q., Huang, Z.-Q., & Shu, F.-W. 2023, *PhRvD*, 107, 084019, doi: [10.1103/PhysRevD.107.084019](https://doi.org/10.1103/PhysRevD.107.084019)
- Loeb, A. 2024, arXiv e-prints, arXiv:2408.10799, doi: [10.48550/arXiv.2408.10799](https://doi.org/10.48550/arXiv.2408.10799)
- Park, R. S., Folkner, W. M., Williams, J. G., & Boggs, D. H. 2021, *AJ*, 161, 105, doi: [10.3847/1538-3881/abd414](https://doi.org/10.3847/1538-3881/abd414)
- Pitjeva, E. V., Pitjev, N. P., Pavlov, D. A., & Turygin, C. C. 2021, *A&A*, 647, A141, doi: [10.1051/0004-6361/202039893](https://doi.org/10.1051/0004-6361/202039893)
- Seto, N., & Cooray, A. 2004, *PhRvD*, 70, 063512, doi: [10.1103/PhysRevD.70.063512](https://doi.org/10.1103/PhysRevD.70.063512)
- Thoss, V., Burkert, A., & Kohri, K. 2024, *MNRAS*, 532, 451, doi: [10.1093/mnras/stae1098](https://doi.org/10.1093/mnras/stae1098)
- Tran, T. X., Geller, S. R., Lehmann, B. V., & Kaiser, D. I. 2023, arXiv e-prints, arXiv:2312.17217, doi: [10.48550/arXiv.2312.17217](https://doi.org/10.48550/arXiv.2312.17217)
- Yalinewich, A., & Caplan, M. E. 2021, *MNRAS*, 505, L115, doi: [10.1093/mnrasl/slab063](https://doi.org/10.1093/mnrasl/slab063)